ELSEVIER

Computational Materials Science 29 (2004) 1–11

COMPUTATIONAL MATERIALS SCIENCE

www.elsevier.com/locate/commatsci

Square representative volume elements for evaluating the effective material properties of carbon nanotube-based composites

X.L. Chen, Y.J. Liu *

Computer-Aided Engineering Research Laboratory, Department of Mechanical Engineering, University of Cincinnati, P.O. Box 210072, Cincinnati, OH 45221-0072, USA

Abstract

Carbon nanotubes (CNTs) demonstrate unusually high stiffness, strength and resilience, and may become an ideal reinforcing material for new nanocomposites. However, much work has to be done before the potentials of CNT-based composites can be fully realized. Evaluating the effective material properties of such nanoscale materials is one of many difficult tasks. Simulations using molecular dynamics and continuum mechanics models can play significant roles in this development. Currently, the continuum approach seems to be the only feasible approach for such large scale analysis. In this paper, effective mechanical properties of CNT-based composites are evaluated using a square representative volume element (RVE) based on the continuum mechanics and with the finite element method (FEM). Formulas to extract the effective material constants from solutions for the square RVEs under two load cases are derived based on the elasticity theory. Numerical results using the FEM show that the load carrying capacities of the CNTs in a matrix are significant. For example, with the addition of CNTs in a matrix at a volume fraction of 3.6%, the stiffness of the composite can increase as much 33% in the axial direction with long CNTs. These simulation results are consistent with the experimental results reported in the literature and the earlier results using cylindrical RVEs.
© 2003 Elsevier B.V. All rights reserved.

Keywords: Carbon nanotubes; Nanocomposites; Effective properties; Finite element method

1. Introduction

Carbon nanotubes (CNTs) possess exceptionally high stiffness, strength and resilience, as well as superior electrical and thermal properties. Many believe that CNTs may provide the ultimate reinforcing materials for the development of a new class of nanocomposites (see, e.g., recent comprehensive reviews [1,2]). It has been demonstrated that with only 1% (by weight) of CNTs added in a matrix material, the stiffness of a resulting composite film can increase between 36% and 42% and the tensile strength by 25% [3]. The mechanical-load carrying capacities of CNTs in nanocomposites have also been demonstrated in some experimental work [3–6] and numerical simulations [7,8]. All these investigations show that the

* Corresponding author. Tel.: +1-513-556-4607; fax: +1-513-556-3390.

E-mail address: yijun.liu@uc.edu (Y.J. Liu).

0927-0256/$ - see front matter © 2003 Elsevier B.V. All rights reserved.
doi:10.1016/S0927-0256(03)00090-9

load-carrying capacities of CNTs in a matrix is significant and the CNT-based composites have the potential to provide extremely strong and ultralight new materials.

However, much work still need to be done before the potentials of the CNT-based composites can be fully realized in real engineering applications. Evaluating the effective material properties of such nanoscale materials is one of the challenging tasks for the development of nanocomposites. Computational approaches, based on the molecular dynamics (MD) approach (for smaller scales) and continuum mechanics approach (for larger scales), can play significant roles in the areas of characterizing CNT-based composites.

The *MD approach* has provided abundant simulation results for understanding the behaviors of individual and bundled CNTs [9–17]. However, MD simulations of CNTs are currently limited to very small length and time scales and cannot deal with the larger length scales in studying nanocomposites. Nanocomposites for engineering applications must expand from nano to micro, and eventually to macrolength scales. Therefore, continuum mechanics models can be applied initially for simulating the mechanical responses of the CNTs in a matrix, as has been done in [7,8] for studying the overall responses of CNT composites, before efficient large multiscale models are established.

The *continuum mechanics approach* has been employed for quite some time in the study of individual CNTs or CNT bundles to investigate their mechanical properties. The validity of the continuum approach to modeling of CNTs is still not fully established and the practice will continue to be questioned for some time to come. However, it seems to be the only feasible approach at present to obtain preliminary results for characterizing CNT-based composites using modeling and simulations. The best argument for using this continuum approach for now is simply the fact that it has been applied successfully for studying single or bundled CNTs, as given in Refs. [18–25]. In these studies, the CNTs are considered as homogeneous and isotropic materials using continuum beam, shell, as well as 3-D solid models in the analyses of the deformation, buckling and dynamics responses of CNTs. Material properties such as equivalent Young's modulus and Poisson's ratios, and buckling modes of CNTs have been successfully predicted by using these continuum approaches. However, cautions should be excised in applying the continuum approach, as discussed in Ref. [7]. Emphasis should be placed on the overall responses of CNTs or CNT-based composites, rather than on the local detailed phenomena, such as interfacial stresses or debonding, where the nanoscale MD approach should be employed. Evaluating the effective materials properties of the CNT-reinforced composites deals with the overall mechanical responses of the RVEs, as presented in Ref. [8] and this paper. Thus, the continuum approach seems adequate for this study, although further development and validation are needed.

The modeling considerations in characterizing CNT-based composites using the continuum approach are discussed in Ref. [7]. It is proposed that the 3-D elasticity models, instead of beam or shell models, should be employed for modeling the CNTs embedded in a matrix, in order to ensure the accuracy and compatibility between the models for the CNTs and matrix. A method based on the elasticity theory for evaluating effective material properties of CNT-based composites using the representative volume elements (RVEs) (Fig. 1) is established and cylindrical RVEs (Fig. 1(a)) are investigated in Ref. [8]. Formulas to extract the effective material properties from numerical solutions for the cylindrical RVEs under three loading cases are derived. Analytical results (extended rule of mixtures) based on the strength of materials theory to estimate the effective Young's modulus in the axial direction, which can help validate the numerical solutions, are also derived for both long and short CNT cases in [8]. Numerical results using the finite element method (FEM) for the cylindrical RVEs show significant increases of the stiffness in the CNT direction of the nanocomposites under various combinations of the CNT and matrix material properties [8]. However, although cylindrical RVEs are easy to use, for which analytical solutions can be derived and efficient 2-D axisymmetric FEM models can be applied, they are the most primitive models and can lead to errors due to ignoring materials not covered by the cylindrical cells.

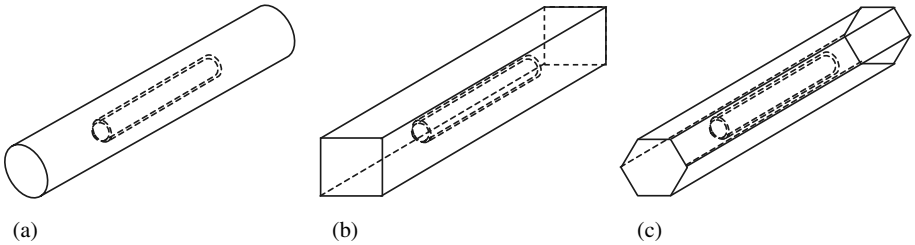

Fig. 1. Three possible RVEs for the analysis of CNT-based nanocomposites [7]. (a) Cylindrical RVE; (b) square RVE; and (c) hexagonal RVE.

In this paper, the work initiated in [8] is extended to *square* RVEs (Fig. 1(b)) for the evaluations of effective material properties of the CNT-based composites. New formulas based on the elasticity theory for extracting the effective material properties from solutions of the square RVEs are derived and numerical studies using the FEM are conducted. Square 2-D RVE models containing multiple CNTs are also investigated for evaluating the effective material constants in the transverse directions. The numerical results from the square RVEs are compared with those obtained earlier using the cylindrical RVEs in [8]. It is found that the cylindrical RVEs tend to overestimate the effective Young's moduli of the CNT-based composites, and the square RVEs may be the preferred models for obtaining more accurate results.

2. Formulas for extracting the effective material constants

To derive the formulas for extracting the equivalent material constants, a homogenized elasticity model of the square RVE (Fig. 2) is considered. The geometry of the elasticity model is corresponding to a solid square RVE with length L and cross-sectional area $2a \times 2a$ (Fig. 3). Elasticity solutions can be obtained under certain load cases. The elasticity model is filled with a single, *transversely isotropic* material that has five independent material constants. The four effective material constants (Young's moduli E_x and E_z, and Poisson's ratios ν_{xy} and ν_{zx}, relating the normal stress and strain components) will be determined (see

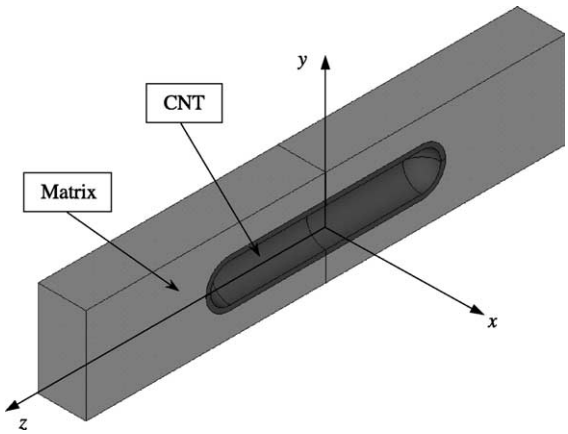

Fig. 2. A square RVE containing a short CNT shown in a cut-through view.

Fig. 2 for the orientation of the coordinates). The fifth independent material constant—the shear modulus G_{xz} $(= G_{yz})$ can be obtained using a simple (torsion) load case and will not be considered in this paper. The general 3-D strain–stress relation relating the *normal* stresses $(\sigma_x, \sigma_y, \sigma_z)$ and strains $(\varepsilon_x, \varepsilon_y, \varepsilon_z)$ for a *transversely isotropic* material can be written as (see, e.g., [26]):

$$\begin{Bmatrix} \varepsilon_x \\ \varepsilon_y \\ \varepsilon_z \end{Bmatrix} = \begin{bmatrix} \frac{1}{E_x} & -\frac{\nu_{xy}}{E_x} & -\frac{\nu_{zx}}{E_z} \\ -\frac{\nu_{xy}}{E_x} & \frac{1}{E_x} & -\frac{\nu_{zx}}{E_z} \\ -\frac{\nu_{zx}}{E_z} & -\frac{\nu_{zx}}{E_z} & \frac{1}{E_z} \end{bmatrix} \begin{Bmatrix} \sigma_x \\ \sigma_y \\ \sigma_z \end{Bmatrix}. \tag{1}$$

To determine the four unknown material constants (E_x, E_z, ν_{xy} and ν_{zx}), four equations will be needed. Two loading cases (Fig. 3) have been devised to provide four such equations based on the elasticity theory, as illustrated below (for comparison, three load cases are needed for the cylindrical RVEs [8]).

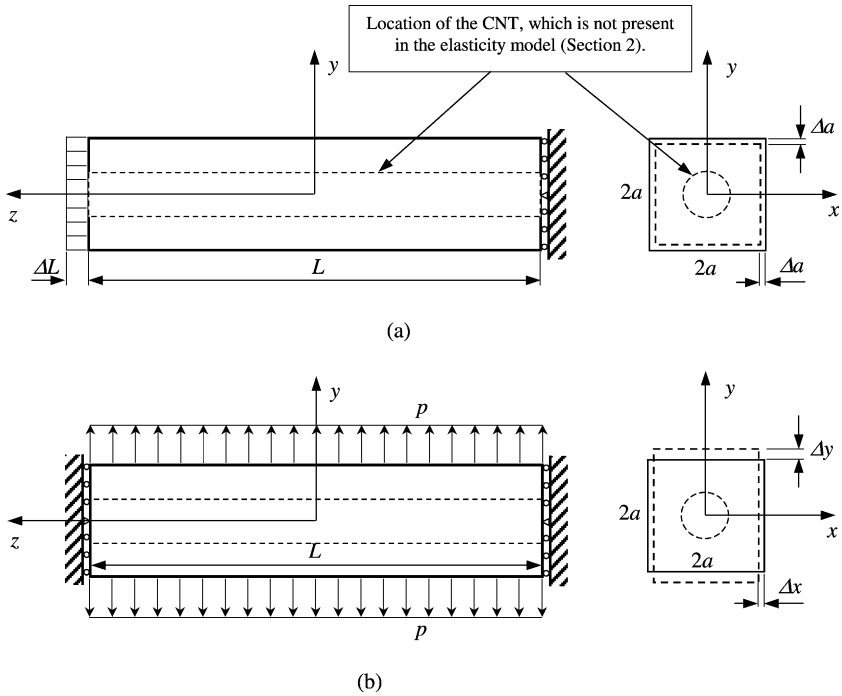

Fig. 3. Two loading cases for the square RVE used to evaluate the effective material properties of the CNT-based composites. (a) Under axial stretch ΔL; and (b) under lateral uniform load p.

2.1. Square RVE under an axial stretch ΔL (Fig. 3 (a))

In this load case (Fig. 3(a)), the stress and strain components on the lateral surface are:

$$\sigma_x = \sigma_y = 0, \quad \varepsilon_z = \frac{\Delta L}{L}, \quad \varepsilon_x = \frac{\Delta a}{a} \text{ along}$$
$$x = \pm a, \quad \text{and} \quad \varepsilon_y = \frac{\Delta a}{a} \text{ along } y = \pm a,$$

where Δa is the change of dimension a of the cross-section under the stretch ΔL in the z-direction ($\Delta a < 0$, if $\Delta L > 0$). Integrating and averaging the third equation in (1) on the plane $z = L/2$, one has immediately:

$$E_z = \frac{\sigma_{\text{ave}}}{\varepsilon_z} = \frac{L}{\Delta L}\sigma_{\text{ave}}, \tag{2}$$

where the averaged value of stress σ_z is given by:

$$\sigma_{\text{ave}} = \frac{1}{A}\int_A \sigma_z(x, y, L/2)\,\mathrm{d}x\,\mathrm{d}y,$$

with A being the area of the end surface. The value of σ_{ave} is evaluated for the RVE using the FEM results.

Using the first (or second) equation in Eq. (1) and the result (2), one has along $x = \pm a$:

$$\varepsilon_x = -\frac{\nu_{zx}}{E_z}\sigma_z = -\nu_{zx}\frac{\Delta L}{L} = \frac{\Delta a}{a}.$$

Thus, one obtains an expression for the Poisson's ratio:

$$\nu_{zx} = -\left(\frac{\Delta a}{a}\right)\Big/\left(\frac{\Delta L}{L}\right). \tag{3}$$

Eqs. (2) and (3) can be applied to estimate the effective Young's modulus E_z and Poisson's ratio ν_{zx} ($= \nu_{zy}$), once the contraction Δa and the stress σ_{ave} in case (a) are obtained.

2.2. Square RVE under a lateral uniform load p (Fig. 3(b))

In this load case (Fig. 3(b)), the square RVE is loaded with a uniformly distributed load (negative

pressure) p in a lateral direction, for example, the y-direction. The RVE is constrained in the z-direction so that the plane strain condition is maintained, in order to simulate the interactions of the RVE with surrounding materials in the z-direction. Since $\varepsilon_z = 0$, $\sigma_z = \nu_{zx}(\sigma_x + \sigma_y)$ for plane strain cases, the 3-D stress–strain relation (1) (for normal components) is reduced to:

$$\begin{Bmatrix} \varepsilon_x \\ \varepsilon_y \end{Bmatrix} = \begin{bmatrix} \frac{1}{E_x} - \frac{\nu_{zx}^2}{E_z} & -\frac{\nu_{xy}}{E_x} - \frac{\nu_{zx}^2}{E_z} \\ -\frac{\nu_{xy}}{E_x} - \frac{\nu_{zx}^2}{E_z} & \frac{1}{E_x} - \frac{\nu_{zx}^2}{E_z} \end{bmatrix} \begin{Bmatrix} \sigma_x \\ \sigma_y \end{Bmatrix}. \tag{4}$$

For the corresponding elasticity model (Fig. 3(b)), one has the following results for the normal stress and strain components at a point on the lateral surfaces:

$$\sigma_x = 0, \quad \sigma_y = p, \quad \varepsilon_x = \frac{\Delta x}{a} \text{ along}$$
$$x = \pm a, \quad \text{and} \quad \varepsilon_y = \frac{\Delta y}{a} \text{ along } y = \pm a,$$

where Δx (<0) and Δy (>0) are the changes of dimensions in the x- and y-direction, respectively, in this load case. Applying the first equation in (4) for points along $x = \pm a$ and the second equation in (4) for points along $y = \pm a$, one has:

$$\varepsilon_x = -\left(\frac{\nu_{xy}}{E_x} + \frac{\nu_{zx}^2}{E_z}\right)p = \frac{\Delta x}{a}, \quad \text{and}$$
$$\varepsilon_y = \left(\frac{1}{E_x} - \frac{\nu_{zx}^2}{E_z}\right)p = \frac{\Delta y}{a},$$

respectively. By solving these two equations, one obtains the effective Young's modulus and Poisson's ratio in the transverse direction (xy plane, Fig. 2):

$$E_x = E_y = \frac{1}{\frac{\Delta y}{pa} + \frac{\nu_{zx}^2}{E_z}}, \tag{5}$$

$$\nu_{xy} = -\left(\frac{\Delta x}{pa} + \frac{\nu_{zx}^2}{E_z}\right) \Big/ \left(\frac{\Delta y}{pa} + \frac{\nu_{zx}^2}{E_z}\right), \tag{6}$$

in which E_z and ν_{zx} have been determined from Eqs. (2) and (3) from load case (a). Once the changes in dimensions, Δx and Δy, are determined for the square RVE from, for example, a finite element analysis, E_x $(= E_y)$ and ν_{xy} can be computed from Eqs. (5) and (6), respectively.

3. Rules of mixtures based on the strength of materials theory

Similar to the cylindrical RVE cases [8], simple rules of mixtures can be established based on the strength of materials theory. These rules of mixtures can be applied to verify the numerical results for the effective Young's moduli in the CNT axial direction. More general theories and extended results, in the context of fiber-reinforced composites, can be found in Refs. [26,27].

3.1. CNT through the length of the RVE (Fig. 4(a))

This is the case when the CNT is relatively long (with large aspect ratio) and therefore a segment can be modeled using an RVE. For the square RVE, the volume fraction [26] of the CNT (a tube, Fig. 4(a)) is defined by:

$$V^t = \frac{\pi(r_o^2 - r_i^2)}{4a^2 - \pi r_i^2}. \tag{7}$$

Following Ref. [8], the effective Young's modulus E_z in the axial direction is found to be:

$$E_z = E^t V^t + E^m(1 - V^t), \tag{8}$$

where E^t is the Young's modulus of the CNT and E^m that of the matrix.

3.2. CNT inside the RVE (Fig. 4(b))

In this case (Fig. 4(b)), the square RVE is divided into two segments: one segment accounting for the two ends with a total length of L_e and Young's modulus E^m; and another segment accounting for the center part with a length of L_c and an *effective* Young's modulus E^c. Note that the two hemispherical end caps of the CNT have been ignored in this simple strength of materials model. For the center part, which is a special case of the one shown in Fig. 4(a), its effective Young's modulus is found to be:

$$E^c = E^t V^t + E^m(1 - V^t), \tag{9}$$

using Eq. (8), in which the volume fraction of the CNT V^t given by Eq. (7) is computed based on the center part of the RVE (with length L_c) only.

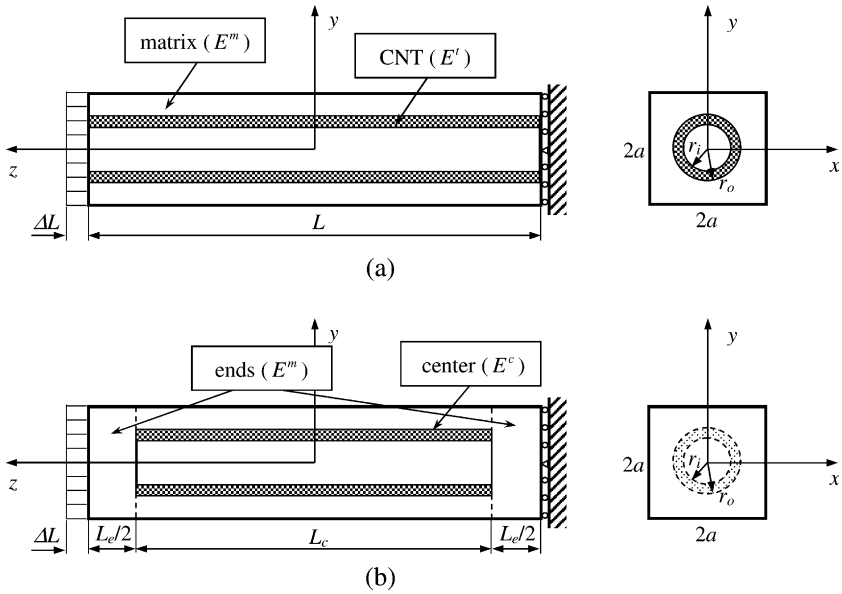

Fig. 4. Simplified strength of materials models based on the square RVEs for estimating the effective Young's modulus E_z in the CNT direction. (a) CNT through the length of the RVE; and (b) CNT inside the RVE ($L = L_e + L_c$).

Again, following Ref. [8], the effective Young's modulus E_z is found to be:

$$E_z = \frac{1}{\frac{1}{E^m}\left(\frac{L_e}{L}\right) + \frac{1}{E^c}\left(\frac{L_c}{L}\right)\left(\frac{A}{A_c}\right)}, \tag{10}$$

which is derived based on the strength of materials theory, in which $A = 4a^2$, $A_c = 4a^2 - \pi r_i^2$ (Fig. 4(b)). This is an *extended rule of mixtures* compared to that given in Eq. (8). Eq. (10) can be employed to estimate the effective Young's modulus for the case shown in Fig. 4(b) when the CNT is relatively short and thus inside the square RVE.

In this paper, Eqs. (8) and (10) will be applied to compare the FEM estimates of the effective Young's moduli in the axial direction in the following section.

4. Numerical examples

Several square RVE models for single-walled CNTs in a matrix material are studied using the FEM in this section, in order to evaluate the effective material constants of the CNT-based nanocomposite. The deformations and stresses are computed first for the two loading cases (Fig. 3) as described in Section 2. The FEM results are then processed, and Eqs. (2), (3), (5) and (6) are applied to extract the effective Young's moduli and Poisson's ratios for the CNT-based composite. Two numerical examples are studied, one on RVEs with long CNTs and the other on an RVE with a short CNT. In all the cases, quadratic solid (brick) elements are employed for the 3-D models and quadratic 8-node elements are used for 2-D plane strain models, both of which offer higher accuracy in FEM stress analysis.

4.1. Long CNTs through the length of a square RVE

First, an RVE for a long CNT all the way through the RVE length, similar to the one shown in Fig. 4(a), is studied. The dimensions are: for the matrix, length $L = 100$ nm, $a = 10$ nm; for the CNT, length $L = 100$ nm, outer radius $r_o = 5$ nm, inner radius $r_i = 4.6$ nm (effective thickness = 0.4 nm, which is close to the theoretical value of 0.34 nm for CNT thickness). The Young's moduli and Poisson's ratios used for the CNT and matrix are:

$$\text{CNT}: \quad E^t = 1000\ \text{nN/nm}^2\ (\text{GPa}), \nu^t = 0.3;$$
$$\text{Matrix}: \quad E^m = 100\ \text{nN/nm}^2\ (\text{GPa}), \nu^m = 0.3.$$

These values of the dimensions and material constants are chosen for illustration purposes only, which are within the wide ranges of those for CNTs reported in the literature [12,15,16,18,28–34]. These parameters can be modified readily for a specific case in future simulations.

First, a full 3-D finite element model containing one CNT is used as shown in Fig. 5. One layer of elements are used for the CNT in this mesh, which have been found to be good enough to obtain converged FEM results. The 3-D FEM model is applied with the two load cases shown in Fig. 3. From the FEM results, the four material constants are extracted using Eqs. (2), (3), (5) and (6).

The results for the effective material constants of the CNT-based composite from the 3-D FEM model are given in Table 1 (first row of data). The effective Young's modulus E_z estimated by the strength of materials solutions is also listed in Table 1 for comparison. The strength of materials solution (Eq. (8)) is identical to that using the FEM, due to the simple geometry and load condition in this case. The results reveal that the increase of the stiffness of the composite can be significant in the CNT axial direction. With a volume fraction of the CNT being only about 3.6%, the stiffness of the composite in the axial direction (E_z) can increase by about 33% compared with that of the matrix, when $E^t/E^m = 10$.

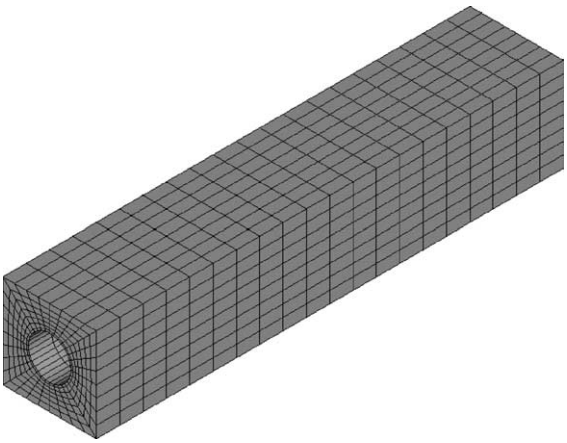

Fig. 5. A 3-D FEM model for the square RVE with a long CNT (CNT thickness = 0.4 nm, with one layer of elements).

Next, two plane strain (2-D) FEM models, containing 5×5 and 10×10 CNTs, respectively, are studied under the lateral loading (Fig. 3(b)). The FEM mesh for the 10×10 CNT model is shown in Fig. 6 and the stress plot is given in Fig. 7, which shows the typical distributions of the stresses around a CNT. The results of the effective Young's modulus and Poisson's ratio in the transverse direction (xy plane, Fig. 2) are listed in Table 1 (second and third rows of data), for which the Young's modulus E_z and Poisson's ratio ν_{zx} needed in Eqs. (5) and (6) are from the above 3-D RVE results. The results from the three models (3-D single CNT, 2-D 5×5 and 10×10 CNT models) are also almost identical as shown in Table 1. This suggests that a single CNT model, either 2-D or 3-D, may be sufficient in determining the effective material constants in the transverse direction, as has been the case in studying conventional fiber-reinforced composites, if the reinforcing fibers (CNTs here) are distributed uniformly in a square pattern in the transverse direction.

For comparison, the effective material constants obtained using the cylindrical RVE from Ref. [8], which is of the same size (same length L and the

Table 1
Computed effective material constants for case (a): long CNT(s) through the RVE

FEM model	E_z/E^m		FEM		
	FEM	RM	ν_{zx}, ν_{zy}	E_x/E^m, E_y/E^m	ν_{xy}
3-D, single CNT	1.3255	1.3255	0.3000	0.8492	0.3799
2-D, 5×5 CNTs	–	–	–	0.8561	0.3745
2-D, 10×10 CNTs	–	–	–	0.8534	0.3745
Cylindrical RVE [8]	1.4384	1.4384	0.3000	1.3336	0.4855

Note: Modulus ratio $E^t/E^m = 10$, CNT thickness = 0.4 nm, volume fraction = 3.617%; RM = rule of mixtures (Eq. (8) for square RVEs; Ref. [8] for cylindrical RVEs).

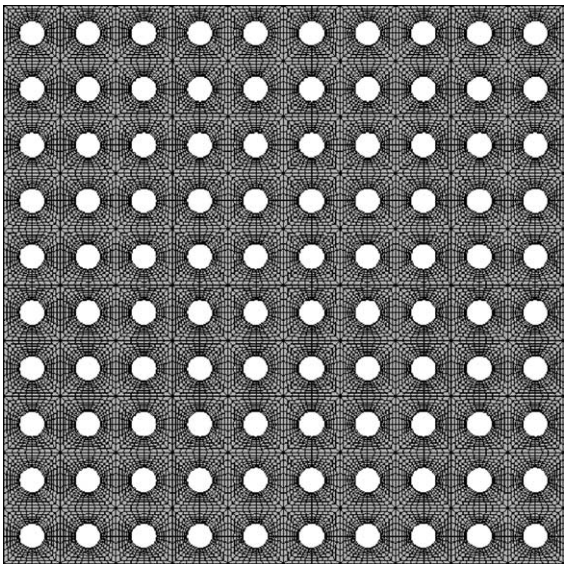

Fig. 6. A 2-D (plane strain) FEM model of the RVE containing 10×10 long CNTs (CNT thickness = 0.4 nm, with one layer of elements).

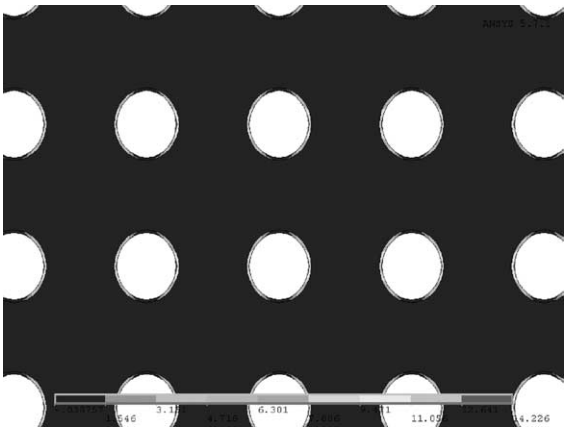

Fig. 7. Plot of the first principal stresses ($\times p$) for the 10×10 RVE model under lateral loading (zoomed in view; $E^t/E^m = 10$).

diameter of the cylindrical RVE $= 2a$ of the square RVE), are also listed in Table 1. It is seen that the cylindrical RVE overestimates the Young's moduli. This may be explained by the fact that a cylindrical RVE overestimates the volume fraction of the CNT due to the negligence of the small amount of matrix material (at the four corners of the square RVE) in the cylindrical RVE.

4.2. A short CNT inside the square RVE

In this example, a square RVE for a short CNT in a matrix, as shown in Fig. 2, is studied. 3-D FEM models has to be employed for this case, even for the lateral loading situation. The dimensions for the RVE are the same as in the previous example, except for the total length of the CNT, which is 50 nm (including the two end hemispherical caps). The material constants used for the CNT and matrix are the same as in the previous example. The finite element mesh used for a quarter symmetry model is shown in Fig. 8. Again, one layer of elements (quadratic bricks) are used through the thickness of the CNT. Coupled DOF constraints are imposed on the four lateral surfaces under both axial and lateral loading (Fig. 3(a) and (b)), so that all points on the lateral surfaces will move the same amount in the normal direction to simulate the constraints from the surrounding material.

Stress contour plots of the first principal stresses in the quarter model of the RVE are shown in Fig. 9 for the axial stretch case and in Fig. 10 for the lateral loading case. The load-carrying capacities of the CNT are obvious from these two stress plots, which are consistent with the earlier simulation results using cylindrical RVEs [7,8]. The computed four effective material constants using the FEM results are shown in Table 2, along with the strength of materials solution (Eq. (10)) for the stiffness in the axial direction (E_z). The increase of

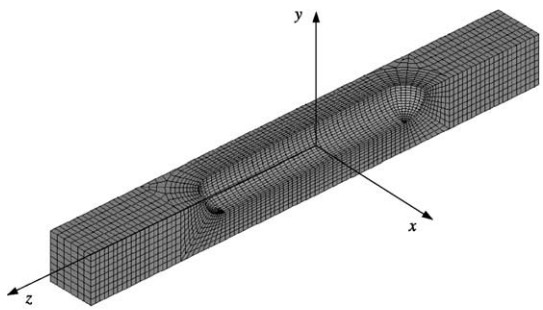

Fig. 8. A 3-D quarter-symmetry FEM model for the square RVE with a short CNT (CNT thickness = 0.4 nm, with one layer of elements).

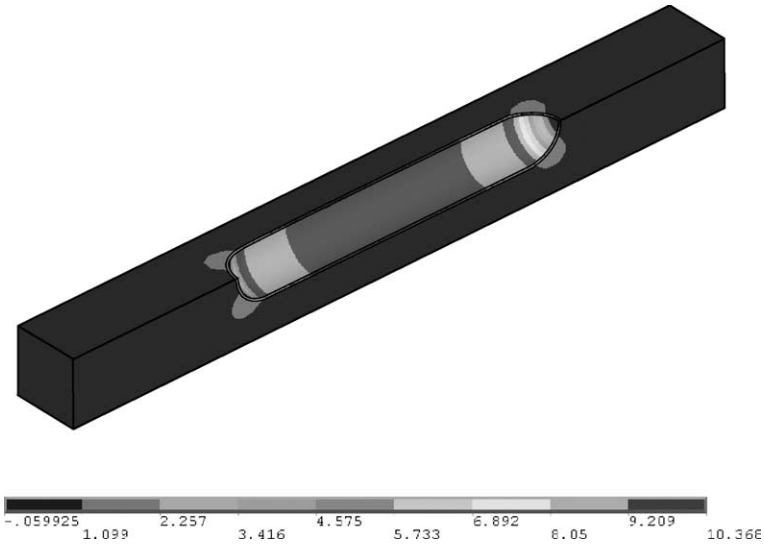

Fig. 9. Plot of the first principal stresses ($\times \Delta L$) for the 3-D RVE under the axial stretch ΔL ($E^t/E^m = 10$).

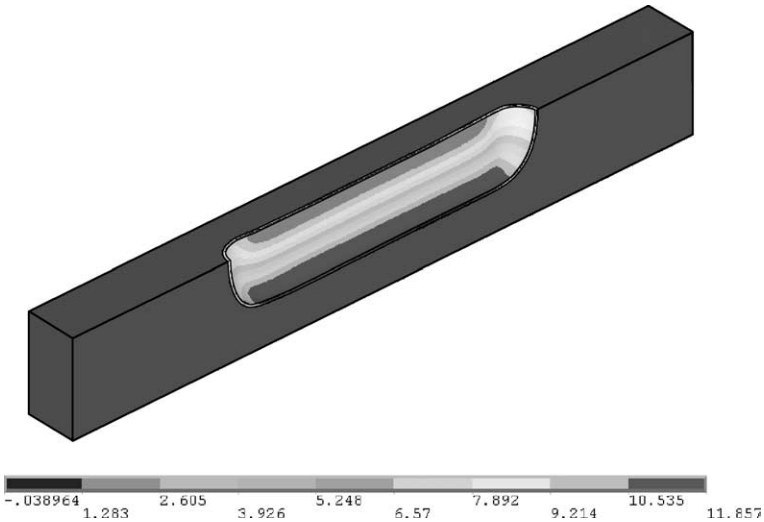

Fig. 10. Plot of the first principal stresses ($\times p$) for the 3-D RVE under the lateral load p ($E^t/E^m = 10$).

the stiffness in the axial direction is moderate for $E^t/E^m = 10$, due to the small volume fraction of the CNT (about 1.6%). These results suggest that short CNTs in a matrix may not be as effective as long CNTs in reinforcing a composite. Again, for comparison, the effective material constants obtained using the cylindrical RVE in Ref. [8] are also listed in Table 2. The cylindrical RVE again overestimates the Young's moduli compared with the current square RVE model.

The strength of materials solution for the stiffness in the axial direction (E_z), using the *extended rule of mixtures* (Fig. 4(b) and Eq. (10)), is quite close to the FEM solution which is based on 3-D elasticity, with a difference of only about 1%. Therefore, the extended rule of mixtures (Eq. (10))

Table 2
Computed effective material constants for case (b): a short CNT inside the RVE

FEM model	E_z/E^m		FEM		
	FEM	ERM	ν_{zx}, ν_{zy}	E_x/E^m, E_y/E^m	ν_{xy}
3-D, single CNT	1.0391	1.0500	0.3009	0.9342	0.3217
Cylindrical RVE [8]	1.0491	1.0628	0.3014	1.0033	0.2614

Note: Modulus ratio $E^t/E^m = 10$, CNT thickness = 0.4 nm, volume fraction = 1.620%; ERM = extended rule of mixtures (Eq. (10) for square RVEs; Ref. [8] for cylindrical RVEs).

may serve as a quick tool to estimate the stiffness of the CNT-based composites in the axial direction when the CNTs are relatively short, while the conventional rule of mixtures (Eq. (8)) can continue to serve in cases when the CNTs are relatively long.

5. Conclusion

The effective mechanical properties of CNT-based composites are evaluated using square RVEs based on 3-D elasticity theory and solved by the FEM. Formulas to extract the effective material constants from solutions for the square RVEs under two loading cases are established based on elasticity. Square RVEs with multiple CNTs are also investigated in evaluating the Young's modulus and Poisson's ratios in the transverse plane. Numerical examples using the FEM are presented, which demonstrate that the load-carrying capabilities of the CNTs in a matrix are significant. With the addition of only about 3.6% volume fraction of the CNTs in a matrix, the stiffness of the composite in the CNT axial direction can increase as much as 33% for the case of long CNT fibers. These simulation results are consistent with both the experimental ones reported in the literature (see, e.g., [3–6]) and the earlier numerical ones using the cylindrical RVEs [8]. It is also found that cylindrical RVEs tend to overestimate the effective Young's moduli due to the fact that they overestimate the volume fractions of the CNTs in a matrix. The square RVEs, although more demanding in modeling and computing, may be the preferred model in future simulations for estimating the effective material constants, especially when multiple CNTs need to be considered. Finally, the rules of mixtures, for both long and short CNT cases, are found to be quite accurate in estimating the effective Young's moduli in the CNT axial direction. This may suggest that 3-D FEM modeling may not be necessary in obtaining the effective material constants in the CNT direction, as in the studies of the conventional fiber-reinforced composites.

Efforts in comparing the results presented in this paper using the continuum approach directly with the MD simulations are underway. This is feasible now only for a smaller RVE of one CNT embedded in a matrix. In future research, the MD and continuum approach should be integrated in a multiscale modeling and simulation environment for analyzing the CNT-based composites. More efficient models of the CNTs in a matrix also need to be developed, so that a large number of CNTs, in different shapes and forms (curved or twisted), or randomly distributed in a matrix, can be modeled. The ultimate validation of the simulation results should be done with the nanoscale or microscale experiments on the CNT reinforced composites.

Acknowledgements

The financial support to the first author (X.L.C.) from the University Research Council of the University of Cincinnati is acknowledged.

References

[1] E.T. Thostenson, Z.F. Ren, T.-W. Chou, Advances in the science and technology of carbon nanotubes and their composites: a review, Composites Science and Technology 61 (2001) 1899–1912.

[2] D. Qian, G.J. Wagner, W.K. Liu, M.-F. Yu, R.S. Ruoff, Mechanics of carbon nanotubes, Applied Mechanical Review 55 (2002) 495–533.
[3] D. Qian, E.C. Dickey, R. Andrews, T. Rantell, Load transfer and deformation mechanisms in carbon nanotube–polystyrene composites, Applied Physics Letters 76 (2000) 2868–2870.
[4] H.D. Wagner, O. Lourie, Y. Feldman, R. Tenne, Stress-induced fragmentation of multiwall carbon nanotubes in a polymer matrix, Applied Physics Letters 72 (1998) 188–190.
[5] L.S. Schadler, S.C. Giannaris, P.M. Ajayan, Load transfer in carbon nanotube epoxy composites, Applied Physics Letters 73 (1998) 3842–3844.
[6] C. Bower, R. Rosen, L. Jin, J. Han, O. Zhou, Deformation of carbon nanotubes in nanotube–polymer composites, Applied Physics Letters 74 (1999) 3317–3319.
[7] Y.J. Liu, X.L. Chen, Continuum models of carbon nanotube-based composites by the BEM, Electronic Journal of Boundary Elements, in press (2003).
[8] Y.J. Liu, X.L. Chen, Evaluations of the effective materials properties of carbon nanotube-based composites using a nanoscale representative volume element, Mechanics of Materials 35 (2003) 69–81.
[9] D. Srivastava, M. Menon, K. Cho, Computational nanotechnology with carbon nanotubes and fullerenes, Computing in Science and Engineering 3 (2001) 42–55.
[10] M. Macucci, G. Iannaccone, J. Greer, J. Martorell, D.W.L. Sprung, A. Schenk, I.I. Yakimenko, K.-F. Berggren, K. Stokbro, N. Gippius, Status and perspectives of nanoscale device modelling, Nanotechnology 12 (2001) 136–142.
[11] J. Han, A. Globus, R. Jaffe, G. Deardorff, Molecular dynamics simulations of carbon nanotube-based gears, Nanotechnology 8 (1997) 95–102.
[12] C.F. Cornwell, L.T. Wille, Elastic properties of single-walled carbon nanotubes in compression, Solid State Communications 101 (1997) 555–558.
[13] S.B. Sinnott, O.A. Shenderova, C.T. White, D.W. Brenner, Mechanical properties of nanotubule fibers and composites determined from theoretical calculations and simulations, Carbon 36 (1998) 1–9.
[14] T. Halicioglu, Stress calculations for carbon nanotubes, Thin Solid Films 312 (1998) 11–14.
[15] G.H. Gao, T. Cagin, W.A. Goddard, Energetics, structure, mechanical and vibrational properties of single-walled carbon nanotubes, Nanotechnology 9 (1998) 184–191.
[16] M. Buongiorno Nardelli, J.-L. Fattebert, D. Orlikowski, C. Roland, Q. Zhao, J. Bernholc, Mechanical properties, defects and electronic behavior of carbon nanotubes, Carbon 38 (2000) 1703–1711.
[17] J.-W. Kang, H.-J. Hwang, Mechanical deformation study of copper nanowire using atomistic simulation, Nanotechnology 12 (2001) 295–300.
[18] E.W. Wong, P.E. Sheehan, C.M. Lieber, Nanobeam mechanics: Elasticity, strength, and toughness of nanorods and nanotubes, Science 277 (1997) 1971–1975.
[19] K. Sohlberg, B.G. Sumpter, R.E. Tuzun, D.W. Noid, Continuum methods of mechanics as a simplified approach to structural engineering of nanostructures, Nanotechnology 9 (1998) 30–36.
[20] S. Govindjee, J.L. Sackman, On the use of continuum mechanics to estimate the properties of nanotubes, Solid State Communications 110 (1999) 227–230.
[21] C.Q. Ru, Column buckling of multiwalled carbon nanotubes with interlayer radial displacements, Physical Review B 62 (2000) 16962–16967.
[22] C.Q. Ru, Axially compressed buckling of a doublewalled carbon nanotube embedded in an elastic medium, Journal of the Mechanics and Physics of Solids 49 (2001) 1265–1279.
[23] D. Qian, W.K. Liu, R.S. Ruoff, Mechanics of C_{60} in nanotubes, Journal of Physical Chemistry B 105 (2001) 10753–10758.
[24] D. Qian, W.K. Liu, R.S. Ruoff, Load transfer mechanism in nanoropes, Composite Science and Technology, in press (2003).
[25] P.S. Das, L.T. Wille, Atomistic and continuum studies of carbon nanotubes under pressure, Computational Materials Science 24 (2002) 159–162.
[26] M.W. Hyer, Stress Analysis of Fiber-Reinforced Composite Materials, first ed., McGraw-Hill, Boston, 1998.
[27] S. Nemat-Nasser, M. Hori, Micromechanics: Overall Properties of Heterogeneous Materials, second ed., Elsevier, Amsterdam, 1999.
[28] R.S. Ruoff, D.C. Lorents, Mechanical and thermal properties of carbon nanotubes, Carbon 33 (1995) 925–930.
[29] M.M.J. Treacy, T.W. Ebbesen, J.M. Gibson, Exceptionally high Young's modulus observed for individual carbon nanotubes, Nature 381 (1996) 678–680.
[30] J.P. Lu, Elastic properties of single and multilayered nanotubes, Journal of Physics and Chemistry of Solids 58 (1997) 1649–1652.
[31] A. Krishnan, E. Dujardin, T.W. Ebbesen, P.N. Yianilos, M.M.J. Treacy, Young's modulus of single-walled nanotubes, Physical Review B—Condensed Matter 58 (1998) 14013–14019.
[32] N. Yao, V. Lordi, Young's modulus of single-walled carbon nanotubes, Journal of Applied Physics 84 (1998) 1939–1943.
[33] C. Goze, P. Bernier, L. Henrard, L. Vaccarini, E. Hernandez, A. Rubio, Elastic and mechanical properties of carbon nanotubes, Synthetic Metals 103 (1999) 2500–2501.
[34] J.P. Salvetat, J.M. Bonard, N.H. Thomson, A.J. Kulik, L. Forro, W. Benoit, L. Zuppiroli, Mechanical properties of carbon nanotubes, Applied Physics A—Materials Science and Processing 69 (1999) 255–260.